

Early-stage clear cell tubulopapillary renal cell carcinoma: imaging features and distinction from clear cell and papillary subtypes

Gevork N. Mnatzakanian,^{1,2} Atul B. Shinagare,^{1,3} V. Anik Sahni,¹ Michelle S. Hirsch,⁴ Stuart G. Silverman¹

¹Department of Radiology, Brigham and Women's Hospital, 75 Francis St, Boston, MA 02115, USA

²Present address: Department of Medical Imaging, St. Michael's Hospital, 3-141CC, 30 Bond St., Toronto, ON M5B 1W8, Canada

³Present address: Dana-Farber Cancer Institute, 450 Brookline Ave, Boston, MA 02215, USA

⁴Department of Pathology, Brigham and Women's Hospital, 75 Francis St., Amory-3, Boston, MA 02115, USA

Abstract

Purpose: Clear cell tubulopapillary renal cell carcinoma (CCTPRCC) is a recently described, low-grade subtype of renal cancer. We determined if imaging features could be used to distinguish early-stage CCTPRCC from stage-matched clear cell RCC (ccRCC) and papillary RCC (pRCC).

Methods: This IRB-approved retrospective study included 54 stage T1a patients with pathologically confirmed CCTPRCC ($n = 18$), ccRCC ($n = 18$), and pRCC ($n = 18$). CT ($n = 48$) and MRI ($n = 27$) exams were reviewed and imaging features compared. Continuous variables were evaluated using ANOVA and Tukey's multiple comparison tests. Categorical variables were compared using Chi-square test or Fisher's exact test.

Results: Compared to pRCC, CCTPRCC had a lower mean attenuation value on unenhanced CT ($p < 0.017$), was more often hyperintense on T2-weighted images ($p < 0.0001$), showed an ill-defined margin ($p = 0.003$), and demonstrated nonenhancing areas ($p = 0.0003$). The presence of all three of these statistically significant features [hypoattenuation (unenhanced attenuation ≤ 25 HU), ill-defined margin, nonenhancing areas] yielded an area under the receiver operator curve (ROC) of 0.92 (95% CI 0.83–0.99) for differentiating

CCTPRCC from pRCC. There were no significant differences in the imaging features of CCTPRCC and ccRCC.

Conclusions: Early-stage clear cell tubulopapillary renal cell carcinoma can be distinguished from papillary RCC based on low attenuation on unenhanced CT, high intensity on T2-weighted images, an ill-defined margin, and presence of nonenhancing areas, but cannot be distinguished from clear cell RCC.

Key words: Clear cell tubulopapillary renal cell carcinoma—Renal cell carcinoma subtype—Renal mass—CT and MRI features

Clear cell tubulopapillary renal cell carcinoma (CCTPRCC) represents a unique subtype of renal epithelial neoplasm according to the recent International Society of Urological Pathology Vancouver Classification of Renal Neoplasia [1, 2]. Also known as 'clear cell papillary renal cell carcinoma' and previously referred to as 'papillary renal cell carcinoma with clear cell features', CCTPRCC is now considered the fourth most common variant of RCC, behind ccRCC (70%), pRCC (16.6%), and chromophobe carcinoma (5.9%), with an incidence of 4.1% [1–6]. CCTPRCC was reported initially in patients with end-stage renal disease; however, the majority of subsequent cases are now known to occur sporadically [1–3, 5–9]. The average age at presentation is 60 and there is no sex predilection [1, 2, 8, 9].

There is limited literature on the biologic behavior of CCTPRCC; however, prior reports suggest that these neoplasms behave indolently, and carry a favorable

This Health Insurance Portability and Accountability Act-compliant retrospective study was performed after approval of the Brigham and Women's institutional review board.

Correspondence to: Gevork N. Mnatzakanian; email: mnatzakanian@smh.ca

prognosis [1–4, 7–10]. To our knowledge, metastases have not been reported [1–4, 7–11]. Therefore, the prospective differentiation of CCTPRCC from the more common subtypes such as clear cell RCC (ccRCC) and papillary RCC (pRCC) at an early stage may be useful for counseling patients on prognosis and treatment plans. For example, an active surveillance approach may be considered in a patient with CCTPRCC [12].

To our knowledge, no prior study has attempted to differentiate CCTPRCC from other renal cell tumor subtypes using imaging features. In a recent study of papillary renal cell carcinoma subtypes on CT and MRI, CCTPRCC was included as an ‘atypical papillary RCC’ and was not evaluated as a separate entity [13]. We determined if imaging features could be used to distinguish early-stage CCTPRCC from stage-matched ccRCC and pRCC.

Methods

Subjects

This Health Insurance Portability and Accountability Act-compliant retrospective study was performed after approval of our institutional review board; informed consent was waived. Our pathology database revealed 23 patients with stage T1a CCTPRCC diagnosed at our institution; of these, 20 had a pretreatment CT scan and/or an MRI examination available for review. Of these 20 patients, two patients had two separate tumors within the same location (upper pole, mid kidney, lower pole), each of which was a different subtype of RCC (including CCTPRCC). Because we were unable to be certain which tumor was CCTPRCC on the images, these two patients were excluded. Thus, a total of 18 patients (9 men, 9 women; median age 65 years; range 43–84) with stage T1a CCTPRCC were included in the study. Of these, 11 were examined with both CT and MRI, six with only CT, and one with only MRI. An equivalent number of consecutive stage-matched ccRCC ($n = 18$; 12 men, six women; median age 56 years; range 22–76) and an equivalent number of consecutive stage-matched pRCC ($n = 18$; 10 men, eight women; median age 64 years; range 50–80) were identified and included to comprise a total of 54 patients in the study.

CT and MRI technique

Of the 54 patients, 27 were examined with CT alone, 21 with both CT and MRI, and six with MRI alone. CT examinations were performed with MDCT scanners (Somatom Volume Zoom, Definition AS 128, Somatom Sensation 64 and 16, all from Siemens Medical Solutions, Erlangen Germany); or Aquilion 320 and Aquilion 64, both from Toshiba (America Medical Systems, Minnetonka, MN). Of the 48 patients who underwent a CT examination, 32 were examined with CT urography, nine

with portal venous phase contrast-enhanced CT, and seven with unenhanced CT. All images were acquired at 120 kVp and 155–280 mA, and reconstructed at 3- to 5-mm-thick sections in the axial plane. For the 32 patients who underwent a CT urogram, contrast-enhanced CT images were obtained 100 s after intravenous injection of 75–120 mL of iopromide (Ultravist 300, Bayer Healthcare, Seattle, WA) for the nephrographic phase. CT urograms were also supplemented with the injection of 10 mg of IV furosemide (Lasix, Abbott Laboratories) administered 2–3 min before contrast material, or supplemented with a drip infusion of 250 mL of IV saline just prior to obtaining the excretory phase images (10–15 min) [14]. For the nine patients who underwent a portal venous phase contrast-enhanced CT, images were acquired 70 s after the injection of 75–120 mL of iopromide. Weight-based dosing was used for all IV contrast material administrations.

MRI examinations were performed on a 1.5-T or 3-T system (Signa Excite 1.5T, GE Healthcare or Magnetom Verio 3T, Siemens Healthcare). Imaging included an axial fat-suppressed T1-weighted spoiled gradient-echo sequence (TR range/TE, 260–435/4.2; flip angle, 75°; section thickness, 4–6 mm; gap, 1 mm; field of view, 34–40 cm) or a 3D fast-acquisition multiple-excitation spoiled gradient-echo sequence [TR range/TE range, 4.4–7.3/1.5–2.2; flip angle, 10°; section thickness, 2.5 mm (effective); gap, 0 mm; field of view, 32–40 cm] before and after IV gadolinium administration [Gadavist (gadobutrol), Bayer Pharmaceuticals, 0.1 mL/kg with maximum dose of 10 mL]. After unenhanced acquisitions, gadolinium-enhanced imaging was performed using delays of 30, 70, 120, and 300 s, respectively. Chemical shift T1-weighted imaging was acquired with a breath-hold spoiled gradient-echo dual-echo in-phase and out-of-phase sequence (TR/TE, 230/2.2–4.4 ms for 1.5 T, 230/1.28–2.46 ms for 3T; flip angle, 90°). T2-weighted imaging was performed with a single-shot fast spin-echo sequence (1200–2500/87–92; number of echoes acquired per TR, 184–264; section thickness, 5 mm; gap, 1 mm; field of view, 32–40 cm) [15]. Respiratory triggered fat-suppressed single-shot echoplanar diffusion-weighted imaging was performed in the transverse plane with tri-directional diffusion gradients by using at least three b values (0, 500, and 1000) within the same acquisition in 10 of the 27 patients who underwent MRI examinations. Of the 27 patients who were examined with MRI, two did not receive IV contrast material due to impaired renal function.

Assessment of imaging features on both CT and MRI

All CT and MRI exams were assessed independently by three abdominal radiologists with 5, 9, and 12 years of experience; each was blinded to the pathologic subtype,

clinical information, and the scores of the other readers. Discrepancies (anything but complete agreement by all three readers) were resolved in consensus. The following imaging features were recorded for all tumors: maximal tumor diameter (mm), tumor location (upper pole, mid kidney, or lower pole), growth pattern (endophytic, <50% exophytic or ≥50% exophytic), tumor margin (well-defined or ill-defined), tumor composition (solid or cystic), appearance on nephrographic phase CT (homogeneous or heterogeneous), attenuation values (HU) on all three phases, signal intensity on T1 (hypo-, iso-, hyperintense to renal cortex), T2 appearance (hypo-, iso-, hyperintense to renal cortex), appearance on diffusion-weighted images (hypo-, iso-, hyperintense to renal cortex), as well as the presence or absence of calcification, central scar, capsule, nonenhancing areas, lesional fat, and lesional hemosiderin.

Maximum tumor diameter was defined as the maximum dimension in the axial plane on nephrographic or excretory phase images [16]. For growth pattern, a tumor was defined as endophytic if the tumor was located completely within the renal parenchyma with no bulge of the capsule [13]. A tumor was considered exophytic if a portion of its margin extended beyond the edge of the renal parenchyma [13]. A tumor margin was considered to be well-defined if >90% of the entire tumor circumference was ‘pencil-thin’ sharp using a narrow window setting [16]. When both nephrographic and excretory phases were available and there was discordance between the two, the phase that showed the most well-defined tumor was used. Regarding tumor composition, a tumor was considered to be cystic when ≥50% of tumor volume was cystic, defined as water attenuation values (≤20 HU) and not enhancing on CT, or being T2 hyperintense and not enhancing on MRI. Tumors with <50% cystic component were considered to be solid [16].

Regions of interest attenuation values were obtained on enhanced CT scans in the portion of the renal mass that revealed the most enhancement as determined subjectively on the axial images. Similar sized regions of interest attenuation values were obtained on the unenhanced CT scans corresponding to the same area of maximal enhancement. Each reviewer independently placed regions of interest and the mean of the three measurements was utilized. Enhancement was calculated by subtracting the high attenuation values of the tumor on unenhanced images from the attenuation value on each of the following phases: nephrographic and excretory. The maximum degree of enhancement was recorded. An increase in attenuation of 20 HU or greater indicated enhancement, an increase of 10–19 HU was considered equivocal, and an increase of <10 HU indicated no enhancement [13, 17–19]. For tumors imaged with MRI, the relative signal intensity in comparison to the normal renal cortex (e.g., hypointense, isointense, hyperintense) was assessed on unenhanced T1, T2, DWI,

and contrast-enhanced T1-weighted images. The presence or absence of enhancement was determined subjectively on subtraction images.

Presence of calcification was assessed only with CT. The presence of a central scar was defined as a central stellate area of T2 hyperintensity with lack of enhancement during the nephrographic phase with or without enhancement during subsequent phases [20]. Nonenhancing areas (assessed for only solid tumors) were defined as hypoattenuating, nonenhancing areas which were not sharply demarcated and lacked apparent walls [16]. Presence of macroscopic fat was defined as a region within the tumor that measured –10 HU or less on CT, or exhibited a loss of signal on fat-saturated T1 images. Presence of intracytoplasmic fat was defined as loss of signal on the opposed phase of the chemical shift imaging sequence. Presence or absence of hemosiderin was only considered for tumors imaged with MRI and defined as the subjective identification of loss of signal intensity on longer-TE in-phase images relative to opposed-phase T1-weighted dual-echo gradient-recalled echo images [13].

Statistical analysis

Stratified analyses of the three subtypes of RCC were conducted. Categorical variables were compared using Chi-square test (gender, side, tumor location, Fuhrman grade, tumor growth pattern, capsule, nonenhancing areas, intralesional fat, central scar, presence of hemosiderin, MRI enhancement, T1, T2, and DWI signal intensities) and Fisher’s exact test (tumor margin, tumor composition, presence of calcification, nephrographic phase appearance, homogeneity/heterogeneity on T1, T2, and DWI). Continuous variables were evaluated using ANOVA and Tukey’s multiple comparison tests (age, tumor size, mean attenuation on unenhanced, nephrographic, and excretory phase). Further pairwise analyses were performed for statistically significant differences. Since three pairwise analyses were performed, using Bonferroni correction, a statistically significant value was determined to be ≤0.017.

Then, the imaging features which were significantly different between the three cancer subtypes were used to construct a receiver operator curve (ROC) to determine the ability of these features to be used to differentiate them. The sensitivity and specificity for differentiating them when one or more of the features were present were calculated also. For this analysis, we assessed the unenhanced CT attenuation value as a binary variable (whether or not the mass was hypoattenuating) and performed a threshold analysis using 5 HU increments starting at 20 HU, and used the lowest attenuation value that yielded a statistically significant difference between the three cancer subtypes. The number of patients did not allow a multivariate analysis to be performed. The number of patients also did not allow assessment of

signal intensity on T2-weighted images to be included in the ROC analysis. Statistical analyses were performed using JMP Pro 11.0.0 (SAS Institute Inc, Cary, NC) and Prism 6 version 6.05 (GraphPad Software Inc, La Jolla, CA).

Results

CCTPRCC demonstrated a lower mean attenuation value on unenhanced CT than pRCC (24.9 HU vs. 33.7 HU; $p < 0.017$) (Fig. 1). However, the mean attenuation value of CCTPRCC (24.9 HU) was not different from that of ccRCC (25.9 HU) ($p > 0.05$) (Table 1). More CCTPRCCs were T2-hyperintense than pRCC ($p < 0.0001$); similarly more ccRCCs were T2-hyperintense than pRCC ($p < 0.002$) (Fig. 2). However, there was no difference in number of T2-hyperintense CCTPRCCs and ccRCCs ($p = 0.330$). More CCTPRCCs had an ill-defined margin than pRCC ($p = 0.003$); however, there was no significant difference when compared to ccRCC ($p = 0.733$) (Fig. 3). Of the 54 tumors, 47 were solid. Among these, both CCTPRCC and ccRCC more frequently demonstrated nonenhancing areas than pRCC ($p = 0.0003$ and 0.0006 respectively), but there was no difference in the frequency of nonenhancing areas between CCTPRCC and ccRCC ($p = 0.990$).

Several imaging features trended toward statistical significance, but pairwise analyses did not reveal a statistically significant difference (Table 1). These included appearance of the tumor on nephrographic phase (ho-

mogeneous vs heterogeneous, $p = 0.033$), appearance on the T1 unenhanced sequences (homogeneous vs heterogeneous, $p = 0.045$), appearance on the T2 sequences (homogeneous vs heterogeneous, $p = 0.045$), and appearance on the DWI sequences (homogeneous vs heterogeneous, $p = 0.007$). There were no significant differences ($p > 0.05$) between CCTPRCC and the other subtypes for the remaining imaging features (Table 1).

The threshold analysis for attenuation values performed for the purpose of ROC analysis yielded a statistically significant unenhanced attenuation value of ≤ 25 HU to differentiate between CCTPRCC and pRCC ($p = 0.03$). An ROC analysis of those features which were significant among the three cancer subtypes demonstrated that the presence of an attenuation value ≤ 25 HU, an ill-defined margin, and the presence of nonenhancing areas could help differentiate CCTPRCC from pRCC with an area under the curve of 0.92 (95% CI 0.83–0.99). When at least one of these features was present, the sensitivity and specificity for diagnosing CCTPRCC were 0.94 and 0.82, respectively. If at least two statistically significant features were present, the sensitivity and specificity for diagnosing CCTPRCC were 0.47 and 1.0, respectively.

Discussion

With the burgeoning role of active surveillance in the management of renal cancer, there is a growing need for ways to help select which patients need prompt treatment and which do not [12, 21]. One way to help select patients

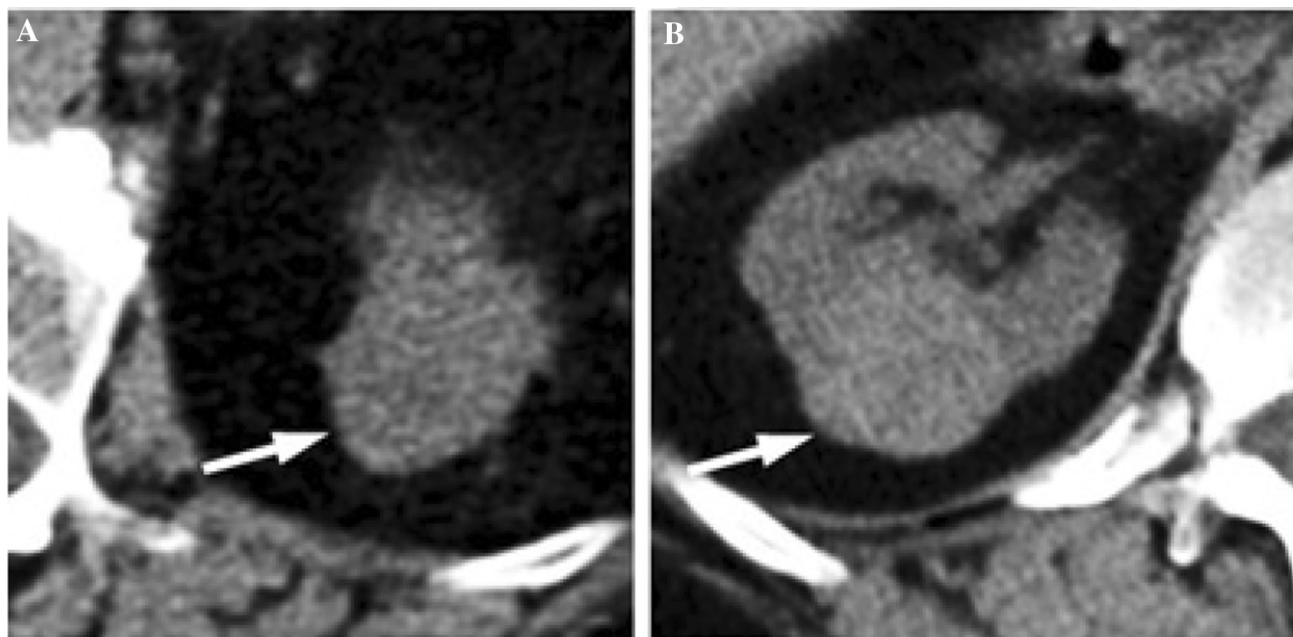


Fig. 1. The mean unenhanced attenuation value of CCTPRCC (24.9 HU) was lower than that of pRCC (33.7 HU). **A** Unenhanced CT of CCTPRCC in an 84-year-old woman

revealed a tumor attenuation value of 14 HU. **B** Unenhanced CT of pRCC in a 61-year-old woman revealed a tumor attenuation value of 51 HU.

Table 1. Imaging features of 54 patients with early-stage clear cell tubulopapillary (CCTPRCC), clear cell (ccRCC), and papillary (pRCC) renal cell carcinoma

Imaging Feature	CCTPRCC (%)	ccRCC (%)	pRCC (%)	<i>p</i> value
Average maximum diameter (mm)	24 (range 13–35 mm)	27 (range 14–39 mm)	25 (range 11–36 mm)	0.465
Side				
Right	11/18 (61)	11/18 (61)	12/18 (67)	0.924
Left	7/18 (39)	7/18 (39)	6/18 (33)	
Location				
Upper	5/18 (28)	9/18 (50)	5/18 (28)	0.274
Mid	7/18 (39)	3/18 (17)	9/18 (50)	
Lower	6/18 (33)	6/18 (33)	4/18 (22)	
Exophytic	16/18 (89)	17/18 (94)	18/18 (100)	0.416
Ill-defined margin	8/18 (44)	6/18 (33)	0/18 (0)	0.003^a
Calcification	3/18 (17)	0/18 (0)	0/18 (0)	0.054
Central scar	0/18 (0)	0/18 (0)	0/18 (0)	1.000
Capsule present	7/18 (39)	5/18 (28)	8/18 (44)	0.574
Solid	14/18 (78)	15/18 (83)	18/18 (100)	0.118
Nonenhancing areas	8/14 (57)	8/15 (53)	0/18 (0)	0.0003^a
Macroscopic fat present	0/18 (0)	0/18 (0)	0/18 (0)	1.000
Microscopic fat present	1/12 (8)	1/6 (17)	0/9 (0)	0.595
Nephrographic phase				
Homogeneous	2/18 (11)	4/18 (22)	8/18 (50)	0.033
Heterogeneous	16/18 (89)	14/18 (78)	8/18 (50)	
Mean unenhanced attenuation (HU)	24.9 (SD ± 9.0)	25.9 (SD ± 6.5)	33.7 (SD ± 11.9)	0.017^a
Mean nephrographic attenuation (HU)	94.8 (SD ± 37.6)	88.6 (SD ± 36.1)	67.9 (SD ± 22.6)	0.639
Mean excretory attenuation (HU)	66.6 (SD ± 36.2)	60.7 (SD ± 16.1)	55.6 (SD ± 22.8)	0.317
Hemosiderin present	0/12 (0)	0/6 (0)	0/9 (0)	1.000
T1 unenhanced signal				
Homogeneous	3/12 (25)	2/6 (33)	7/9 (78)	0.045
Heterogeneous	9/12 (75)	4/6 (67)	2/9 (22)	
T1 unenhanced signal				
Hypointense	6/12 (50)	3/6 (50)	0/9 (0)	0.079
Isointense	6/12 (50)	3/6 (50)	8/9 (89)	
Hyperintense	0/12 (0)	0/6 (0)	1/9 (11)	
T2 signal				
Homogeneous	1/12 (8)	0/6 (0)	4/9 (44)	0.045
Heterogeneous	11/12 (92)	6/6 (100)	5/9 (56)	
T2 signal				
Hypointense	0/12 (0)	1/6 (17)	9/9 (100)	0.0001^a
Isointense	1/12 (8)	0/6 (0)	0/9 (0)	
Hyperintense	11/12 (92)	5/6 (83)	0/9 (0)	
DWI signal				
Homogeneous	0/4 (0)	0/4 (0)	2/2 (100)	0.007
Heterogeneous	4/4 (100)	4/4 (100)	0/2 (0)	
DWI signal				
Hypointense	0/4 (0)	1/4 (25)	0/2 (0)	0.435
Isointense	0/4 (0)	0/4 (0)	0/2 (0)	
Hyperintense	4/4 (100)	3/4 (75)	2/2 (100)	
Enhancement present on MRI	11/11 (100)	6/6 (100)	8/8 (100)	1.000

SD = standard deviation

^a Bold numbers denote statistically significant results

for active surveillance is to predict their tumors' biological behavior on the basis of histologic subtype. There are emerging data to suggest that RCC subtypes may be diagnosed with imaging [22, 23]; however, currently this distinction and the subsequent clinical management decision often rely on pathology obtained at biopsy.

CCTPRCC is a recently recognized subtype of renal cell carcinoma [1, 2] that has gross morphologic and histologic features which overlap with both ccRCC and pRCC [1–9, 11]. In the radiology literature, CCTPRCC has been considered among atypical pRCC subtypes [13], and to our knowledge, the imaging features of this recently described RCC subtype have not been de-

scribed. Almost all (>95%) of CCTPRCCs are stage T1a and do not demonstrate local invasion [1–9, 11]. There are no reported cases of metastases or disease-related deaths [1–11]. In one study, none of 12 patients with stage T1a or T1b CCTPRCC who were followed (mean 19 months) showed local disease progression or developed a metastasis [4]; a similar favorable outcome has recently been published in two larger series of CCTPRCC [5, 6]. Therefore, relative to the more common clear cell and papillary subtypes, CCTPRCC is considered an indolent cancer and may be appropriate to observe rather than treat in selected patients [4, 11].

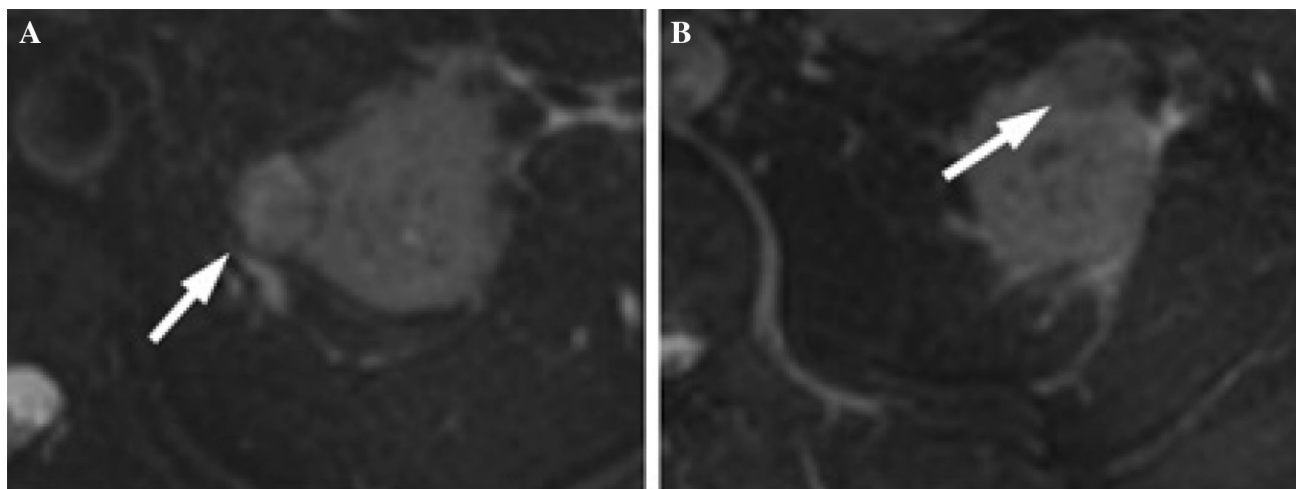


Fig. 2. More CCTPRCCs were T2-hyperintense than pRCC. **A** T2-weighted MRI of CCTPRCC in a 65-year-old man demonstrates heterogeneously hyperintense signal.

B T2-weighted MRI of pRCC in a 52-year-old man demonstrates homogeneously hypointense signal.

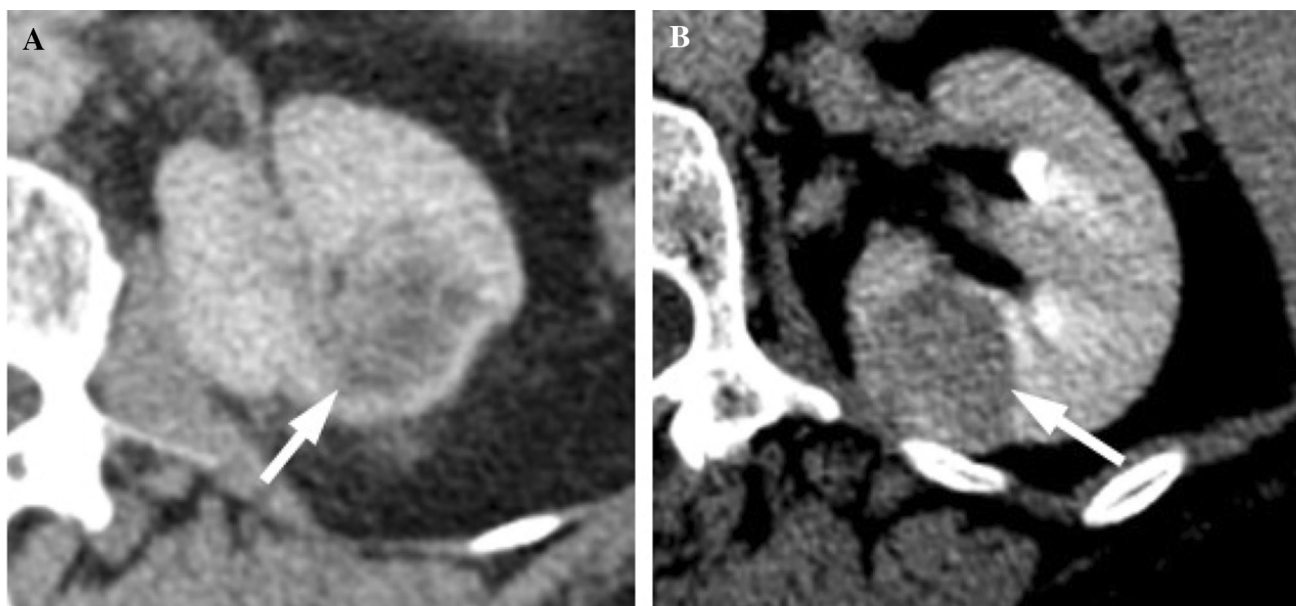


Fig. 3. More CCTPRCCs had an ill-defined margin than pRCC. **A** Contrast-enhanced CT of CCTPRCC in a 75-year-old woman demonstrates an ill-defined tumor margin. **B**

Contrast-enhanced CT of pRCC in a 64-year-old man demonstrates a well-defined tumor margin.

Our study shows that early-stage CCTPRCC typically presents as a solid enhancing neoplasm with a low attenuation on unenhanced CT and a high signal on T2-weighted MR imaging (Fig. 4).

Our comparative analysis suggests that early-stage CCTPRCC can be distinguished from pRCC based on a lower mean attenuation value on unenhanced CT, high signal on T2-weighted images, an ill-defined margin, and more frequent nonenhancing areas. Specifically, a threshold unenhanced attenuation of 25 HU was found to be statistically significant for dif-

ferentiating CCTPRCC from pRCC. This corroborates earlier works which demonstrated that early-stage pRCC is typically hyperattenuating on unenhanced CT [13, 15]. In contrast, the relatively low attenuation appearance for CCTPRCC can be explained by its pathology: CCTPRCC can include cystic components of various sizes [1–3, 7–9]. In fact, in the first description of CCTPRCC, 33 (92%) of 36 tumors included cystic components that often contained serosanguinous fluid or colloid-like secretions [1].

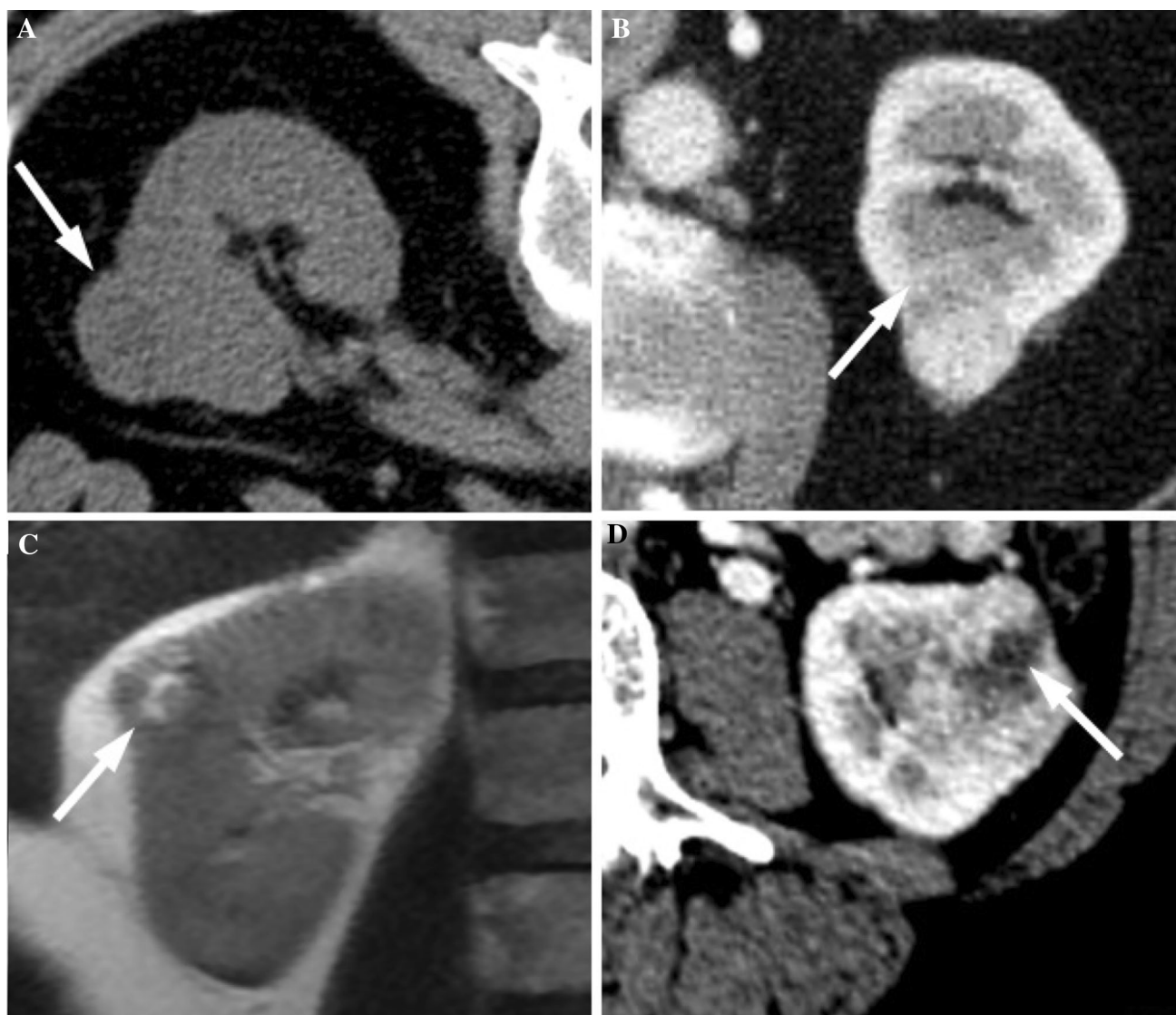


Fig. 4. Common imaging features of CCTPRCC. **A** Unenhanced CT of CCTPRCC in a 53-year-old man demonstrates the tumor has a low attenuation appearance relative to renal cortex. **B** Contrast-enhanced CT of CCTPRCC in a 69-year-old woman demonstrates that the tumor has an ill-defined

margin. **C** T2-weighted MRI of CCTPRCC in a 59-year-old woman demonstrates that the tumor is T2 hyperintense compared to renal cortex. **D** Contrast-enhanced CT of CCTPRCC in a 76-year-old man demonstrates an eccentric nonenhancing area within the tumor.

The cystic nature of most of these tumors also probably explains why CCTPRCC was T2-hyperintense. It is difficult to postulate why CCTPRCC would exhibit an ill-defined margin relative to pRCC. Perhaps due to their hybrid nature, this feature may mimic ccRCC, which has been shown to demonstrate ill-defined margins on imaging [16, 17]. The higher frequency of nonenhancing areas was another feature that could be used to distinguish CCTPRCC from pRCC. Indeed, 8 (57%) of 14 solid CCTPRCC exhibited nonenhancing areas. These data are similar to Egbert et al. [13] who described nonenhancing areas in two of six patients with CCTPRCC. Although others have used nonenhancement in solid masses as an imaging surrogate for tumor necrosis [16, 17], CCTPRCC

typically does not demonstrate necrosis at histologic evaluation [2, 3]. The nonenhancing areas may represent focal fibrosis, colloid or glycogen in the cells, focal cystic change, or necrosis [1–3, 5].

In practical terms, when encountering a small renal mass, our data allow radiologists to include CCTPRCC in the differential diagnosis of neoplastic etiologies, and to favor it along with ccRCC when a mass measures less than or equal to 25 HU on an unenhanced CT scan, is T2-hyperintense, or exhibits ill-defined margins, or nonenhancing areas. The presence of two of these features increases the specificity for differentiating between CCTPRCC and pRCC, but the increased specificity comes at the cost of lowering the sensitivity. The finding

that CCTPRCC cannot be differentiated from ccRCC is supported by several pathology studies that have described CCTPRCC as a mimicker of ccRCC [1–3, 11]. For example, pathologists may have difficulty distinguishing CCTPRCC from ccRCC with a low Fuhrman grade [1, 2, 4], and rely on immunohistochemistry to render the correct diagnosis [1–4, 7–9, 11, 24].

This study had several limitations. First, the number of patients was overall small because the tumor has been only recently described. To our knowledge, this study is the largest series of CCTPRCC in the radiological literature. Second, the study was retrospective; however, the readers were blinded to each patient's pathologic diagnosis in order to minimize bias. Third, both CT and MRI were not available for all patients. However, all patients (except for seven patients whose CT included only an unenhanced phase) were examined using protocols that included integral components for renal mass imaging, image acquisitions before and after intravenous contrast material administration, and reconstructions with 3–5 mm section thickness [12]. Third, we did not include other RCC subtypes in our analysis for two reasons. The two subtypes we chose to compare to CCTPRCC, ccRCC and pRCC, comprise approximately 95% of all renal cell carcinomas. Therefore, our results can be applied to the vast majority of renal cell carcinomas encountered in clinical practice. Moreover, these two entities are the most likely subtypes to appear similar to this new entity. Finally, we were unable to evaluate the contributions of diffusion-weighted imaging; these pulse sequences were not used consistently. In the future, diffusion-weighted imaging may prove useful.

In summary, CCTPRCC is a relatively recently described entity that can be included in the differential diagnosis of renal neoplasms and can be distinguished from pRCC but not ccRCC. Therefore, since CCTPRCC and ccRCC typically behave differently, more work will be needed before management decisions such as active surveillance can be made on the basis of imaging features alone. Additional imaging research may be helpful; in addition to diffusion-weighted imaging, IV contrast material dynamics, shown to distinguish other renal neoplasm subtypes [22, 23, 25–28] may help distinguish CCTPRCC from ccRCC. Nevertheless, the results of our analysis could serve as the foundation for additional studies on the use of imaging to differentiate the recently described CCTPRCC from other RCC subtypes. Finally, a radiology–pathology correlation study would help understand the pathologic correlates of the imaging features of these subtypes.

Compliance with ethical standards

Conflict of interest The author declares that they have no competing interests.

Ethical approval The study was approved by Hospital Institutional Review Board and this constitutes as ethical approval.

References

1. Srigley JR, Delahunt B, Eble JN, et al. (2013) The International Society of Urological Pathology (ISUP) Vancouver classification of renal neoplasia. *Am J Surg Pathol* 37(10):1469–1489
2. Aydin H, Chen L, Cheng L, et al. (2010) Clear cell tubulopapillary renal cell carcinoma: a study of 36 distinctive low-grade epithelial tumors of the kidney. *Am J Surg Pathol* 34(11):1608–1621
3. Montironi R, Mazzucchelli R, Scarpelli M, Lopez-Beltran A, Cheng L (2013) Update on selected renal cell tumors with clear cell features. With emphasis on multilocular cystic clear cell renal cell carcinoma. *Histol Histopathol* 28(12):1555–1566
4. Zhou H, Zheng S, Truong LD, et al. (2014) Clear cell papillary renal cell carcinoma is the fourth most common histologic type of renal cell carcinoma in 290 consecutive nephrectomies for renal cell carcinoma. *Hum Pathol* 45:59–64
5. Aron M, Chang E, Herrera L, et al. (2015) Clear cell-papillary renal cell carcinoma of the kidney not associated with end-stage renal disease: clinicopathologic correlation with expanded immunophenotypic and molecular characterization of a large cohort with emphasis on relationship with renal angiomyoadenomatous tumor. *Am J Surg Pathol* 39:873–888
6. Deml KF, Schildhaus HU, Comperat E, et al. (2015) Clear cell papillary renal cell carcinoma and renal angiomyoadenomatous tumor: two variants of a morphologic, immunohistochemical, and genetic distinct entity of renal cell carcinoma. *Am J Surg Pathol* 39:889–901
7. Gobbo S, Eble JN, Grignon DJ, et al. (2008) Clear cell papillary renal cell carcinoma: a distinct histopathologic and molecular genetic entity. *Am J Surg Pathol* 32(8):1239–1245
8. Adam J, Couturier J, Molinié V, Vieillefond A, Sibony M (2011) Clear-cell papillary renal cell carcinoma: 24 cases of a distinct low-grade renal tumour and a comparative genomic hybridization array study of seven cases. *Histopathology* 58(7):1064–1071
9. Rohan SM, Xiao Y, Liang Y, et al. (2011) Clear-cell papillary renal cell carcinoma: molecular and immunohistochemical analysis with emphasis on the von Hippel-Lindau gene and hypoxia-inducible factor pathway-related proteins. *Mod Pathol* 24(9):1207–1220
10. Tickoo SK, dePeralta-Venturina MN, Harik LR, et al. (2006) Spectrum of epithelial neoplasms in end-stage renal disease: an experience from 66 tumor-bearing kidneys with emphasis on histologic patterns distinct from those in sporadic adult renal neoplasia. *Am J Surg Pathol* 30(2):141–153
11. Liddell H, Mare A, Hewood S, Bennett G, Chan HF (2015) Clear cell papillary renal cell carcinoma: a potential mimic of conventional clear cell renal carcinoma on core biopsy. *Case Rep Urol*. doi:10.1155/2015/423908
12. Silverman SG, Israel GM, Trinh QD (2015) Incompletely characterized incidental renal masses: emerging data support conservative management. *Radiology* 275(1):28–42
13. Egbert ND, Caoili EM, Cohan RH, et al. (2013) Differentiation of papillary renal cell carcinoma subtypes on CT and MRI. *AJR* 201(2):347–355
14. Silverman SG, Akbar SA, Morteale KJ, et al. (2006) Multi-detector row CT urography of normal urinary collecting system: furosemide versus saline as adjunct to contrast medium. *Radiology* 240(3):749–755
15. Oliva MR, Glickman JN, Zou KH, et al. (2009) Renal cell carcinoma: t1 and t2 signal intensity characteristics of papillary and clear cell types correlated with pathology. *AJR* 192(6):1524–1530
16. Shinagare AB, Vikram R, Jaffe C, et al. (2015) Radiogenomics of clear cell carcinoma: preliminary findings of The Cancer Genome Atlas-Renal Cell Carcinoma (TCGA-RCC) Imaging Research Group. *Abdom Imaging* 40(6):1684–1692
17. Israel GM, Silverman SG (2011) The incidental renal mass. *Radiol Clin N Am* 49(2):369–383
18. Silverman SG, Israel GM, Herts BR, Richie JP (2008) Management of the incidental renal mass. *Radiology* 249(1):16–31
19. Chung EP, Herts BR, Linnell G, et al. (2004) Analysis of changes in attenuation of proven renal cysts on different scanning phases of triphasic MDCT. *AJR* 182(2):405–410
20. Rosenkrantz AB, Hindman N, Fitzgerald EF, et al. (2010) MRI features of renal oncocytoma and chromophobe renal cell carcinoma. *AJR* 195:W421–W427

21. Sun M, Abdollah F, Bianchi M, et al. (2012) Treatment management of small renal masses in the 21st century: a paradigm shift. *Ann Surg Oncol* 19(7):2380–2387
22. Lee-Felker SA, Felker ER, Tan N, et al. (2014) Qualitative and quantitative MDCT features for differentiating clear cell renal cell carcinoma from other solid renal cortical masses. *AJR* 203(5):W516–W524
23. Young JR, Margolis D, Sauk S, et al. (2013) Clear cell renal cell carcinoma: discrimination from other renal cell carcinoma subtypes and oncocytoma at multiphasic multidetector CT. *Radiology* 267(2):444–453
24. Williamson SR, Eble JN, Cheng L, Grignon DJ (2013) Clear cell papillary renal cell carcinoma: differential diagnosis and extended immunohistochemical profile. *Mod Pathol*. 26:697–708
25. Ruppert-Kohlmayr AJ, Uggowitz M, Meissnitzer T, Ruppert G (2004) Differentiation of renal clear cell carcinoma and renal papillary carcinoma using quantitative CT enhancement parameters. *AJR* 183:1387–1391
26. Zhang J, Lefkowitz RA, Ishill NM, et al. (2007) Solid renal cortical tumors: differentiation with CT. *Radiology* 244:494–504
27. Sun M, Ngo L, Genega EM, et al. (2009) Renal cell carcinoma: dynamic contrast-enhanced MR imaging for differentiation of tumor subtypes-correlation with pathologic findings. *Radiology* 250(3):793–802
28. Bata P, Gyebnar J, Laszlo D, et al. (2013) Clear cell renal cell carcinoma and papillary renal cell carcinoma: differentiation of distinct histological types with multiphase CT. *Diagn Interv Radiol* 19:387–392